Laser Plasma Interaction in the Shock Ignition Scenario - PIC Modeling

O. Klimo[1,2], S. Weber[2], V. T. Tikhonchuk[2], J. Limpouch[1]

[1]*Czech Technical University in Prague, FNSPE, Brehova 7, 11519, Prague, Czech Republic*

[2]*Centre Lasers Intenses et Applications, Univ. Bordeaux 1-CEA-CNRS, 33405 Talence, France*

Shock Ignition (SI) [1] is considered as a relatively robust way to achieve efficient fuel burn in the inertial confinement fusion (ICF). The phases of the fuel assembly and ignition are separated as in Fast Ignition, but the additional energy to ignite the target is supplied to the central hot spot by a strong converging shock. This shock is launched at the end of the compression phase by an additional ignition laser pulse with the power of the order of hundreds of TW. The ignition laser pulse intensity is thus so high that nonlinear phenomena in the laser plasma interaction, which may undermine the SI efficiency, cannot be avoided. The stimulated scattering instabilities, the Raman and the Brillouin scattering (denoted SRS and SBS respectively), are of particular importance in this context as they are responsible for the absorption and reflection of the laser light and for the acceleration of electrons. These processes are studied in this paper using numerical simulations.

The fully kinetic collisionless simulations are performed using our massively parallel relativistic electromagnetic PIC code in one-dimensional geometry and they are sufficiently long (several tens of ps) so that a quasi-steady state may be established in the interaction. Numerical heating is suppressed by using high order particle shapes. Specially designed absorbing boundary conditions at the rear side of the simulation box allowed us to evaluate correctly the number of hot electrons and the energy transported to denser plasma [2].

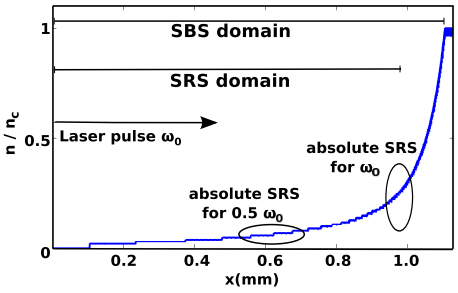

Figure 1: The density profile used in our PIC simulations. The two important regions of absolute SRS instabilities are marked up.

The simulations of the laser plasma interactions for the shock ignition conditions consider realistic parameters of the plasma (temperature, density profile, ion mass) and of the laser pulse (intensity, wavelength) used in recent Omega experiments [3]. The initial density profile of plasma is plotted in Fig. 1. It is taken from hydrodynamic simulations [4] and it can be bound by two exponential curves with the density scale lengths of 100 and 200 μm. The temperatures of electrons and ions taken from [4] are 2.3 and 0.9 keV respectively. The deuteron ions are employed, but the charge to mass ratio corresponds also to an average ion of the plastic shell used in the experiments. The laser pulse has a 5 ps long linear ramp at the beginning and than it

stays on the maximum intensity , which is in the range $10^{15} - 10^{16}$ W/cm^2, until the end of the simulation. The laser wavelength of 350 nm is assumed.

The stimulated scattering instabilities in the context of SI have been described and analyzed in details in our recent paper [2]. They correspond to the laser intensity 10^{16} W/cm^2, wavelength 0.35 μm, the plasma temperature of 5 keV, and the density scale length of 300 μm. Our new results corresponding to the conditions of the Omega experiment with the ignition pulse intensity 5×10^{15} W/cm^2 and the wavelength of 0.35 μm are presented below.

The temporal evolution of the frequency spectrum of the reflected light and the reflectivity are plotted in Fig. 2. One can distinguish three signals in different frequency ranges, which appear successively, in the order from the highest to the lowest frequency. The strongest signal is observed at about the laser frequency ω_0 and it is due to SBS. The Brillouin scattering starts to grow almost immediately, when the rising edge of the laser pulse penetrates into the plasma. The SBS scattered light comes in a series of short intense bursts, which are responsible for the high reflectivity at the beginning of the interaction.

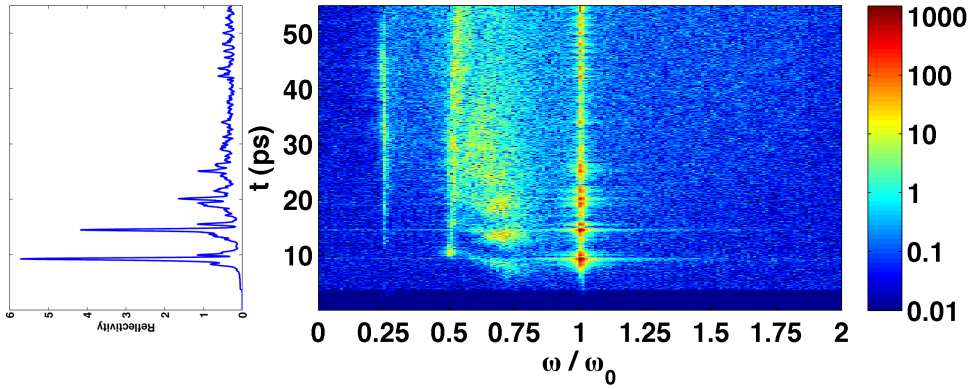

Figure 2: The temporal evolution of the spectral energy density (in arbitrary units). The signals due to SBS near the laser frequency ω_0, SRS at 0.5 ω_0 originated from 1/4th n_c and secondary SRS at 0.25 ω_0 originated from 1/16th n_c can be distinguished. Additional broad feature near 0.7 ω_0 could be related to the forward SRS of the SBS light.

The signal in the vicinity of 0.5 ω_0 is due to Stimulated Raman Scattering (SRS), which takes place in particular near the quarter critical density (n_c) as an absolute instability. Due to a very high plasma temperature Landau damping prevents the occurrence of SRS below 1/4th of n_c. The threshold of SRS is of the same order as the threshold of SBS ($\simeq 10^{14}$ W/cm^2) and thus this instability quickly grows after the laser penetrates up to the quarter critical density. The strong SRS scattered light from the quarter critical density induces another absolute SRS instability at 1/16th of n_c during its propagation from the plasma. This process (so called, Raman cascade) manifests itself by the weak signal in the frequency spectrum at about 0.25 ω_0. Last but not least, there is a relatively strong signal in a broad frequency range around 0.7 ω_0. This part of the spectrum has not been discussed in [2]. Preliminary explanation is that this light comes

from forward SRS of the SBS scattered light. The forward SRS is not suppressed by Landau damping and as the light intensity in the SBS scattered bunches is relatively high, the forward SRS growth rate may become relatively high. A temporal correlation between the SBS radiation and this new signal confirms this assertion. This process will be studied in future.

The absolute Raman scattering instabilities at 1/4th and 1/16th n_c are accompanied by cavitation. Due to the absolute nature of the SRS instability, the field in these regions may become so high that the radiation pressure exceeds the thermal pressure of surrounding plasma. This results in development of deep density cavities. The absolute SRS instabilities at 1/4th and 1/16th n_c and the cavitation processes are responsible for relatively large collisionless absorption. This can be seen in Fig. 3, which demonstrates the evolution of the electromagnetic energy density in time and space. The energy density in this figure is particularly high in the regions around 0.6 and 1 mm, which correspond to the densities of 1/4th and 1/16th n_c. Only a small part of energy can propagate deeper into the target up to critical density. The intense flashes of SBS scattered light are also clearly identified in the left side of Fig. 3 during the first 25 ps. They are originated in the region of 0.5 - 0.9 mm and are amplified propagating in the backward direction.

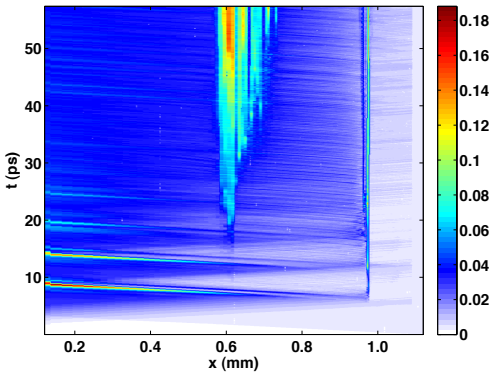

Figure 3: Evolution of the electromagnetic field energy density in time and space. The SBS scattered light and the concentration of the field energy density in the regions of cavities can be observed.

As noted above, most of the laser pulse energy is absorbed in the regions of 1/4th and 1/16th of n_c by collisionless processes related to SRS. As a result of this absorption process, hot electron population is created, which transports the energy deeper into the target. For the optimization of SI efficiency, it is important to characterize the dependence of laser absorption and hot electron temperature on the ignition pulse intensity. With this goal, we conducted two additional simulations at laser intensities 10^{15} and 10^{16} W/cm^2 for the same plasma parameters. The energy distributions of hot electrons transporting the absorbed laser energy into the target are shown in Fig. 4 panel a). The dependence of the hot electron temperature on the ignition pulse intensity is included in panel b). As can be seen, the temperature depends almost linearly on the laser pulse intensity and in the case of the lowest intensity, the population of hot electrons is not clearly distinguishable.

The laser absorption due to the above described processes is ranging between 60% and 66% and thus there is no significant dependence on the laser pulse intensity in the range 10^{15} –

10^{16} W/cm^2. This energy is transported beyond the critical density with fast electrons. The collisions should further increase this relatively high absorption in particular in the case of the lowest intensity.

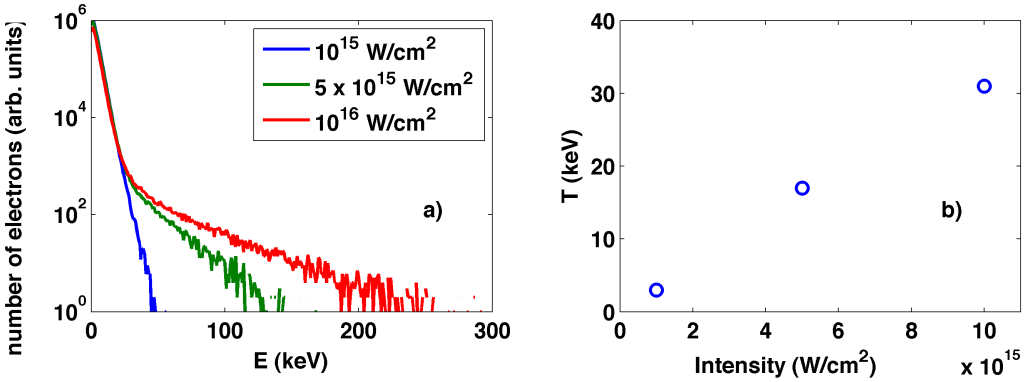

Figure 4: The energy distribution of electrons propagating into the target (panel a) and the dependence of hot electron temperature on the laser pulse intensity (panel b).

We present large scale plasma fully kinetic simulations of the laser plasma interactions for the conditions of recent SI experiments [3]. Our results demonstrate that a high temperature, large scale plasma could provide an efficient collisionless absorption of high intensity laser radiation. The laser energy is absorbed in density cavities that are created and maintained by two coupled SRS processes forming a self-organized resonator between the zones of 1/4th and 1/16th of the critical density. This particular plasma response is due to the high initial plasma temperature that suppresses the SRS development everywhere in plasma with exception of the resonant point. These results are indicating rather favorable conditions for SI, as a relatively large absorption coefficient and a Maxwellian spectrum of hot electrons with a moderate temperature are favorable for creation of high amplitude shock wave in the fusion target. Collisional absorption may become important in the case of lower laser pulse intensities.

Acknowledgments

This work was performed within the framework of the HiPER project. The support by the Czech Ministry of Education, Youth and Sports under project No. LC528 is acknowledged. The authors are grateful to the French national computational center GENCI for the support within the framework of the project KITSI, number x2009056129.

References

[1] R. Betti *et al.*, Phys. Rev. Lett. **98**, 155001 (2007).

[2] O. Klimo *et al.*, Plasma Phys. Control. Fusion **52**, 055013 (2010).

[3] W. Theobald *et al.*, Plasma Phys. Control. Fusion **51**, 124052 (2009).

[4] X. Rybeire, private communication, hydrodynamic simulations of experiments [3].